J. Chem. Sci. (2020) 132:133
https://doi.org/10.1007/s12039-020-01829-7
© Indian Academy of Sciences

REGULAR ARTICLE

Polymorph of *trans*-dichlorotetrakis(pyridine-*N*)ruthenium(II) influenced by a dihydrazone: crystal structure, spectral, Hirshfeld surfaces, antimicrobial, toxicity and *in silico* docking studies

DEBAJANI BASUMATARY[a,*], MADAN KUMAR SHANKAR[b], KULLAIAH BYRAPPA[c], KANDARPA KUMAR SAIKIA[d], AJAZ AHMAD DAR[e], VEDANT VIKROM BORAH[d], PRANJIT SARMA[a], PRANAMI MAHANTA[a], MRITUNJAYA ASTHANA[f] and NAMRATHA KEERTHIRAJ[g]

[a]Department of Applied Sciences, Gauhati University, Guwahati 781 014, India
[b]Institution of Excellence, Vijnana Bhavan, University of Mysore, Mysuru 570 006, India
[c]Research and Innovations Center, Adichunchanagiri University, B.G. Nagara, Mandya 571 448, India
[d]Department of Bioengineering and Technology, Gauhati University, Guwahati 781 014, India
[e]Department of Chemistry, Indian Institute of Technology Guwahati, Guwahati 781 039, India
[f]TCG Lifesciences Pvt. Ltd, Salt Lake, Kolkata 700 091, India
[g]Department of Studies in Earth Science, Manasa Gangotri, University of Mysore, Mysuru 570 006, India
E-mail: debbasumatary@gmail.com; debbasumatary@gauhati.ac.in

MS received 11 March 2020; revised 5 June 2020; accepted 9 June 2020

Abstract. Many reports describe the influence of additives or impurities on the physicochemical properties of crystals. On having obtained *trans*-[$RuCl_2(C_5H_5N)_4$] as brown, needle-shaped crystals contrary to red or orange-red blocks reported previously, we herein revisit its study. This complex was obtained from the filtrate of an ensuing reaction mixture of $RuCl_3{\cdot}3H_2O$, bis(2-hydroxy-l-naphthaldehyde)adipoyldihydrazone ($npahH_4$) and pyridine in methanol. Findings from X-ray crystallographic data and spectra of IR, UV-Visible, ^1H and ^{13}C NMR along with other analytical studies of the complex are presented here. A comparative study with previously reported crystal forms was performed to understand the accompanying molecular structural differences in the physical (shape, size and color) morphological alteration. Further probing into molecular dynamics, the molecular interactions were analyzed and quantified using computational methods. The symmetry of intermolecular interaction in C—H···Cl is different from earlier reported crystal forms. The intercontact H···H showed a major contribution (62.9%) for Hirshfeld surfaces. Also, we report antibacterial activity of the complex against methicillin-resistant *Staphylococcus aureus* followed by the *in silico* docking study that revealed its interaction with the residue Glu58 of ATPase subunit of *S. aureus* GyrB. Additional studies on its toxicity using rat models revealed this complex as non-toxic to animals.

Keywords. Crystal-color morphology; characterization; packing interactions; additive.

1. Introduction

The changes in physical characteristics of a crystal due to additives, impurities, solvent, supersaturation, polymorphism, etc., have been a subject of significant interest and extensive study.[1–9] The physical morphological differences may have an immense impact on the crystal properties like stability, solubility, packing, compaction, mechanical, chemical, electrical, etc.,[2,3] thus, altering the compound's characteristics. So certainly, the physical morphological variations can pave a way to change the compounds behavior for functional applications, such as for designing drugs and materials with desired characteristics.[10] However, crystallization being a complex phenomenon, the current understanding of its underlying mechanism is still rudimentary. There are many reports in the literature that have described the presence of additives or

*For correspondence

Electronic supplementary material: The online version of this article (https://doi.org/10.1007/s12039-020-01829-7) contains supplementary material, which is available to authorized users.

Published online: 25 September 2020

impurities in reactions that were effective in incorporating changes in morphology and properties of the crystals.[4–7] Weissbuch *et al.*[1,8] had monitored the crystallization of α-glycine, which was obtained with a larger plane in the presence of D-alanine while with L-alanine in solution, the crystal exhibited large faces. Similarly, Hendriksen *et al.*[1,9] observed change in crystal morphology of paracetamol with *p*-acetoxyacetanilide (PAA) as an additive. Interestingly, our work intended to synthesize ruthenium complexes of bis(2-hydroxy-1-naphthaldehyde)adipoyldihydrazone from reaction of $RuCl_3{\cdot}3H_2O$ with the ligand in presence of pyridine with methanol as solvent, we obtained crystalline *trans*-$[RuCl_2(C_5H_5N)_4]$ (**C2**) on slow evaporation of filtrate solution at room temperature. The title complex is well-known and is used in many reactions as a starting material or its derivatives are used for the synthesis of ruthenium complexes and as catalysts.[11–18] Ligand $npahH_4$ has been reported in our earlier works[19–21] (Figure 1c). The crystals of **C2** were obtained as brown, thick and rigid needles (Figure 1a) that were studied with single-crystal X-ray crystallography. Subsequently, on comparison of crystal data of **C2** with the previous reports,[22–25] it was notably found to have been obtained as orange-red or red crystals with block morphology in the earlier studies by Wong *et al.*,[22] Elsegood *et al.*,[23] Bu *et al.*[24] and Trivedi *et al.*[25] (Table 1). This prompted us to investigate any structural differences exhibited in the geometries such as bond lengths, angles, other crystal parameters and molecular interactions of the present inadvertently formed complex **C2** from the previously reported crystal forms of *trans*-$[Ru^{II}Cl_2(py)_4]$, resulting in the essential change in morphology. Following this, we have attempted to understand the experimental conditions that may have contributed and facilitated the variation of **C2** rendering its color and crystal morphological change, and as the prerequirement to understand the changes associated with physicochemical characteristics is understanding the fundamentals at the molecular level which was done by collection of basic data from different investigations. We carried out a few different analytical, spectroscopic and computational studies to comprehend the structure analysis. To understand the commonalities and differences in these crystal forms at the molecular level, the intercontacts were examined and analyzed from the important X-ray crystallographic data and substantiated by the powerful methodology of Hirshfield surfaces. Ruthenium compounds are known to have significant pharmacological profiles with remarkable low cytotoxicity,[26,27] so the complex was evaluated for antibacterial activity against bacterial species, namely Gram-positive *S. aureus* and Gram-negative *Escherichia coli* and *Klebsiella pneumoniae*. The complex displayed efficacy against *S. aureus* which is known to have emerged as an antibiotic-resistant bacteria over the last decade mainly due its resistant action to methicillin, [28] so further, the docking studies for the complex were performed with ATPase subunit of *S. aureus* GyrB. Thereafter, the cytotoxicity of this complex was also evaluated in laboratory rats. Accordingly, here we report that the crystal and color polymorphism in **C2** probably is largely induced by the incidental presence of another molecule in the medium functioning as an impurity or additive along with investigations by spectral and single-crystal X-ray analysis to understand its structural differences from crystal forms of past reports. In addition to these, new findings obtained from the studies of other analytical, Hirshfeld surfaces, antibacterial activity, toxicity and molecular docking simulations are presented here.

2. Experimental

2.1 *Materials*

All reagents used in the synthesis of the complex are commercially available and were used without further purification. $RuCl_3{\cdot}3H_2O$, diethyl adipate, hydrazine hydrate and 2-hydroxy-1-naphthaldehyde were of E-Merck grade.

2.2 *Measurements*

Melting point and decomposition temperature were investigated using Analab Scientific Instrument. Infrared spectrum was recorded on a Bomen DA-8FT-IR spectrophotometer in the spectral range 4000–450 cm^{-1} with samples in the form of KBr pellets. Electronic spec-trum was measured on a Perkin Elmer Lambda 25 UV/Vis spectrophotometer in the range 800–250 nm using chloroform solution and 1-cm cell. ^1H NMR and ^{13}C NMR spectra were recorded on a Varian, Mercury Plus 600 MHz NMR spectrophotometer in $CDCl_3$ solutions using TMS as an internal reference. Molar conductance of the complex was measured on a Conductivity-304 with a dip-type conductivity cell at 10^{-3} M in chloroform at room temperature.

2.3 *Synthesis and crystallization of trans-dichlorotetrakis(pyridine-N)ruthenium(II)*

Bis(2-hydroxy-1-naphthaldehyde)adipoyldihydrazone ($npahH_4$) was prepared according to the procedure reported earlier (Figure 1c).[19–21]

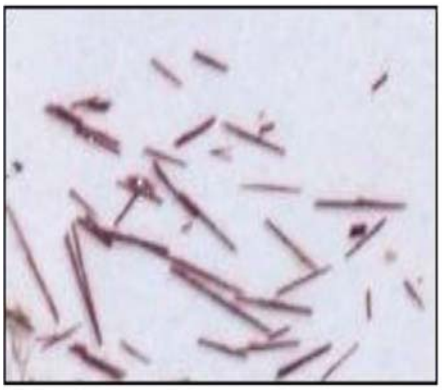

(a)

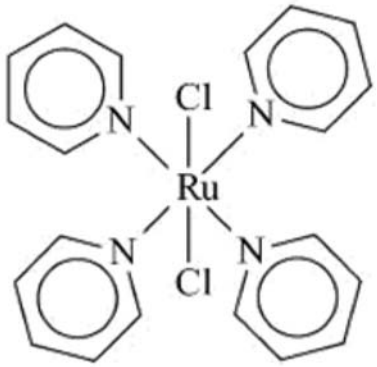

(b)

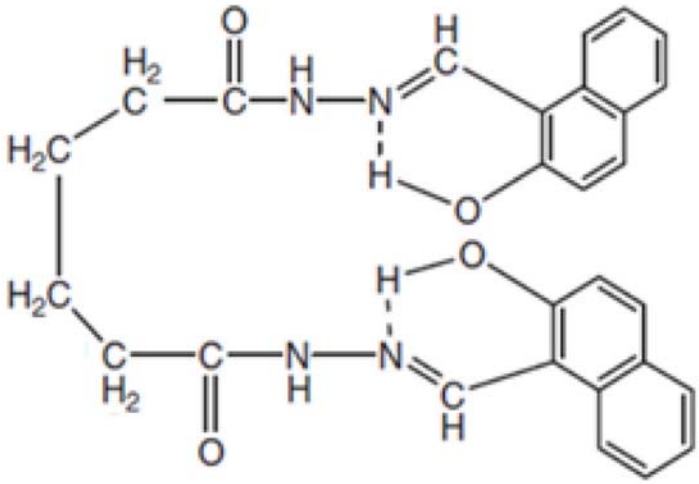

(c)

Figure 1. (a) Brown needle-shaped crystals, (b) schematic drawing of *trans*-[$RuCl_2(py)_4$] and (c) schematic drawing of bis(2-hydroxy-1-naphthaldehyde)adipoyldihydrazone ($npahH_4$).

Table 1. Color and shape comparisons of the reported *trans*-dichlorotetrakis(pyridine-*N*)ruthenium(II) crystals.

CSD refcode	Crystal morphology
This work	Brown and needle
WIBNIE[22]	Orange-red and block
WIBNIE01[23]	Red and block
WIBNIE02[24]	Red and block
WIBNIE03[25]	Red and block

To synthesize the ruthenium complex of ligand bis(2-hydroxy-1-naphthaldehyde)adipoyldihydrazone, $RuCl_3 \cdot 3H_2O$ (0.3813 g, 1.45 mmol) in 20 mL methanol was added to $npahH_4$ (0.708 g, 1.44 mmol) in 20 mL methanol at 1:1 molar ratio and stirred for 10 min at 50°C. This homogeneous reaction mixture was then added with pyridine (1.144 g, 14.45 mmol) maintaining the molar ratio at 1:1:10 of $RuCl_3 \cdot 3H_2O$: $npahH_4$: pyridine. This was refluxed for 1 h, cooled to room temperature, and then filtered. Both precipitate and filtrate were collected. Further, the filtrate solution was kept at room temperature for slow evaporation for several days when crystalline, brown, long and thick needles were observed. These crystals obtained were between 1–12 mm in length with a maximum thickness of 0.5–1.2 mm that were of good quality and suitable for X-ray diffraction analysis (Figure 1a).

The greyish-brown precipitate isolated had a yield of ~63%. After carrying out different analytical studies, it was found to have a composition of $[Ru^{II}(npahH_4)(py)_2]Cl_2$.[21]

2.4 *Analytical studies*

Yield: 22%; M.P. > 300°C; IR (cm^{-1}, KBr): 3690-3630 (sbr), 3436 (s), 3233 (w), 2961 (w), 2924 (w), 2853 (w),

1623 (s), 1479 (w), 1445 (w), 1261 (w), 1190 (w), 1107 (s), 1017 (m), 800 (w), 759 (w), 691 (w), 620 (w), 557 (w), 492 (w); UV-Vis (λ_{max} in nm, ε in $M^{-1}cm^{-1}$ in $CHCl_3$): ~550–572 (60), ~454–464 (100), 397 (400), 275 (970); ^{1}H NMR (δ/ppm, 600 MHz, $CDCl_3$, 298.8 K): 8.57 (d, 8H, J = 5.4 Hz), 7.65 (t, 4H, J = 7.2 Hz), 7.11 (t, 8H, J = 6.3 Hz); ^{13}C NMR (δ value in ppm, $CDCl_3$, 299.8 K): 157.52, 133.85, 123.07; Δ_M at 25 °C ($\Omega^{-1}cm^{-2}$ mol^{-1} in $CHCl_3$): 46.

2.5 *Single-crystal X-ray diffraction*

Crystal data, data collection and structure refinement[29] details are summarized and given in S1 and S2, Supplementary Information. Single-crystal X-ray diffraction data for the complex at 296 K were collected with Mo Kα radiation (λ = 0.71073 Å) using a Bruker Smart Apex II CCD diffractometer equipped with a graphite monochromator. SMART software was used for data collection and also for indexing the reflections and determining the unit cell parameters. Collected data were integrated using SAINT software. The structure was solved by direct methods and refined by full-matrix least-square calculations using SHELXTL software.[30] Absorption corrections were done by the multi-scan method (SADABS). All the non-H atoms were refined in the anisotropic approximation against F^2 of all reflections. The H atoms were placed at their calculated positions and refined in isotropic approximations. The computer programme Mercury was used for generating packing diagram and analyzing the molecular interactions (Table 2).[31] The ORTEP and packing diagram of **C2** are shown in Figure 2, a&b, respectively.

The crystals of **C2** with molecular formula, $C_{20}H_{20}Cl_2N_4Ru$ are tetragonal. At 296 K, a = b = 15.7254 (11) Å, c = 16.9830 (14) Å, V = 4199.7 (7) Å^3, M_r = 488.37, Z = 8, space group = $I4_1/acd$, μ(Mo $K\alpha$) = 1.01 mm^{-1}, crystal size (mm) = 0.52 × 0.15 × 0.12; data collection: absorption correction = multi scan, T_{min}, T_{max} = 0.833, 0.886, no. of measured, independent and observed [$I > 2\sigma(I)$] reflections = 16582, 1544, 1074, R_{int} = 0.022, $(\sin\theta/\lambda)_{max}$ = 0.705 Å^{-1}; refinement: $R[F^2 > 2\sigma(F^2)]$, $wR(F^2)$, S = 0.030, 0.106, 1.00, no. of reflections = 1529, No. of parameters = 78, H-atom treatment = H atoms treated by a mixture of independent and constrained refinement, $\Delta\rho_{max}$, $\Delta\rho_{min}$ (e Å^{-3}) = 0.36, −0.37.

2.6 *Hirshfeld surfaces*

The Hirshfeld surfaces computational method is performed to quantify short contacts in the crystal structure. This method is a graphical tool for exploring and visualization of intermolecular interactions.[32–34] The final coordinates obtained from a single-crystal X-ray diffraction was used as input for the Crystal Explorer. The percentages of inter-contacts are quantified and the Hirshfeld visualizations (2D-fingerprint plots) are shown in Figure 3. The Hirshfeld surfaces are highlighted by conventional mapping of d_{norm} on molecular Hirshfeld surfaces. The electrostatic potential is mapped on Hirshfeld surface using wave function STO-3G basis set at Hartree-Fock theory over the range of ± 0.030 au.[35]

2.7 *Biological activity*

2.7a *Antimicrobial activity*: The complex **C2** was tested for antibacterial activity against Gram-negative bacteria (*E. coli* and *K. pneumoniae*) and Gram-positive (*S. aureus*) bacteria which are some of the most commonly found circulating bacteria in the region. These clinical isolates were chosen from a repository where the antibiotic resistance profile (Table 3 and Figure 4) and the corresponding phenotypic characterization was carried out (data not shown here). Well diffusion and micro-broth dilution assays were carried out to test antibacterial activities. Both well diffusion and broth microdilution assays serve as verifiable methods to assess antibacterial activity; former being an effective method to assess the possible antibacterial activity while the latter is easy, reliable and reproducible[36] to establish the findings from the preliminary investigation (S3, Supporting Information).

2.7b *Toxicity studies*: The acute oral toxicity tests of the complex were also performed, the details are presented in S4 and S5, Supplementary Information.

2.7c *Docking studies*:

(i) *Ligand preparation*: The three-dimensional ligand structure of **C2** was prepared, protonation states were assigned and low-energy three-dimensional conformations were generated with CORINA.[37]

(ii) *Protein preparation*: The three dimensional coordinated derived from a single-crystal structure in X-ray of ATPase subunit of *S. aureus* GyrB (ATP*Sa*, PDB ID-5CTW) with 1.48 Å resolution was obtained from the Protein Data Bank (http://www.rscpdb.org/pdb). The hydrogen atoms were added and water molecules were removed. The ligand (2-(butanoylamino)thiophene-3-carboxamide) was extracted while other species ((4S)-2-methyl-2,4-pentanediol, chlorine and magnesium) was kept for docking. The ligand is defined for the binding site using GOLD Suite.[38] Goldscore was used to identify the best pose of the ligand.

(iii) *Molecular docking:* In the PDB file, the hydrogen atoms were added and water molecules were removed. The extracted ligand was kept as the reference for binding site definition. The binding cavity was defined on the ligands presented in the binding pocket of ATP*Sa*, the atoms or residues within the range of 6 Å around the ligand (reference) were defined for the binding site. The standard settings of the genetic algorithm in GOLD were used. The Goldscore was used for rendering docking solutions.[38]

3. Results and Discussion

3.1 *Crystal description*

C2 crystals are brown in color, thick and long needle-shaped, different from the previously reported orange-red or red block structures. It has crystallized in the tetragonal system (I4(1)/acd space group) similar to past reports. On comparing the geometries (bond lengths, bond angles and torsion angles) with the previous reports,[22–25] no appreciable variations were observed. Nuanced differences in bond lengths of Ru-N and Ru-Cl were between 0.002–0.007 Å and 0.004–0.006 Å, respectively (see Table S2d, Supplementary Information). A list exhibiting comparisons and differences in selected bond lengths and angles of **C2** with earlier reported crystal data collected at a temperature of 293 or 296 K are given in Table S2d, Supporting Information. Few selected bond lengths, bond angles and torsional angles of the complex are listed in S2 and Table S2, a–c, Supplementary Information.

In **C2** crystal structure, intra-molecular C1—H1···Cl1 and inter-molecular C4—H4···Cl1 hydrogen bonds are observed (Table 2). These two intra-molecular and inter-molecular interactions generate a double-helical motif (Figure 2b) and this pattern is same as in the previous reports. The symmetry of intermolecular interaction in C—H···Cl of the present **C2** crystal structure is 1/4-y,1/4-x,9/4-z that is different from the symmetry 1/4-y,1/4-x,1/4-z of the previously reported crystal packing structures. The geometry of this interaction is almost same in all the listed structures of Table 1.[22–25]

3.2 *Hirshfeld surfaces analysis*

The Hirshfeld surfaces of **C2** are shown in Figures 3(i and ii), highlighted by conventional mapping of d_{norm} on molecular Hirshfeld surfaces. The intercontacts (and its 2D fingerprint plot) quantified using Hirshfeld surfaces method are C···C (5.7%, Figure 3b), C···H (17.6%, Figure 3c), Cl···H (13.8%, Figure 3d) and H···H (62.9%, Figure 3e). The percentage of H···H contribution for Hirshfeld surface is abundant in the molecule showing that they play a pivotal role in stabilizing it. The complete intercontact is shown in Figure 3(a). The electrostatic potential over the Hirshfeld surfaces are plotted, the blue region (positive electrostatic potential) over the surface represents the hydrogen donor potential, whereas the hydrogen bond acceptors are represented by red region (negative electrostatic potential) (Figure 3, iii&iv).

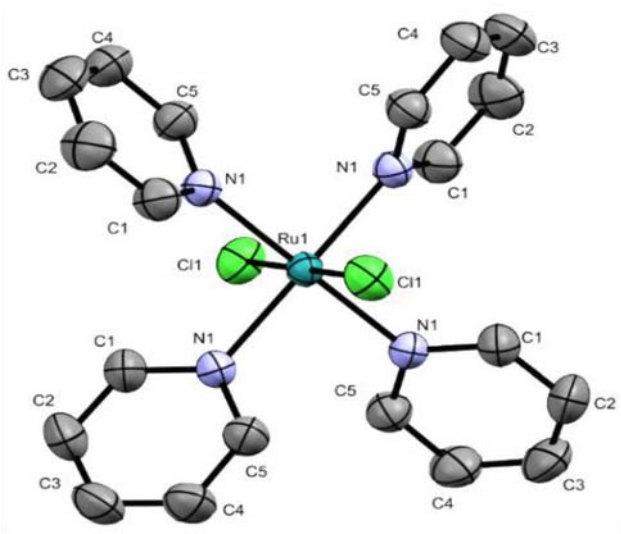

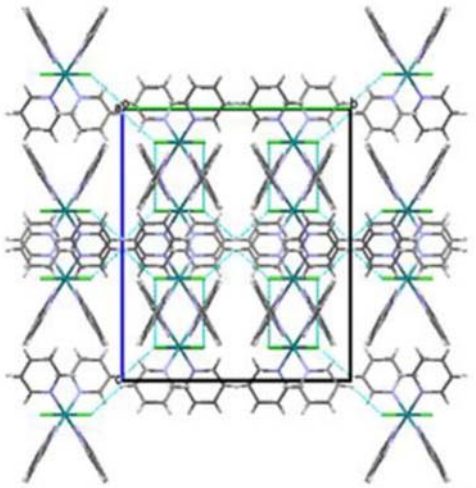

Figure 2. (a) The molecular structure of the complex showing the atom-numbering scheme of non-hydrogen atoms. Displacement ellipsoids are plotted at the 50% probability level. (b) Packing of title molecules along *a*-axis.

Table 2. Hydrogen-bond geometry (Å, °) for complex **C2**.

D—H—A	D—H	H—A	D—A	D—H
Cl—H1···Cl1^{i}	0.93	2.80	3.526(7)	111
C4—H4···Cl1^{ii}	0.93	2.90	3.80(7)	134.96

Symmetry codes: ^{i}1/4-y,1/4-x,9/4-z; ^{ii}1/4-y,1/4-x,9/4-z.

3.3 *Analytical and spectral studies*

It is also interesting that many other earlier studies[11,13,15–18,39,40] had reported yellow, yellow-brown,

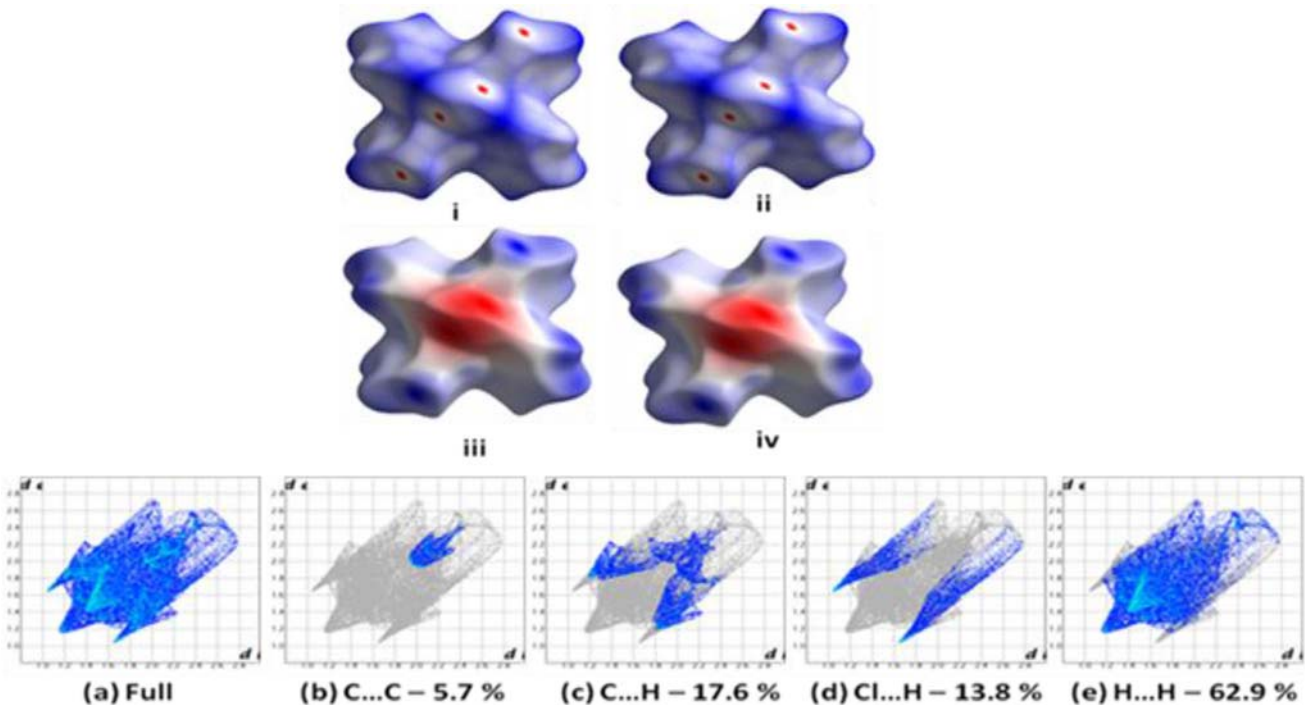

Figure 3. Hirshfeld surfaces and their corresponding 2D fingerprint plots: (i) and (ii) - d_{norm} mapped on the Hirshfeld surface (different orientations) for visualizing the intercontacts of the compound. Color scale in between –0.21 au (blue) – 1.2 au (red). In the 2D fingerprint plot (a–e), *di* is the closest internal distance from a given point on the Hirshfeld surface and *de* is the closest external contacts. The outline of the full fingerprint is shown in gray. The plots iii and iv represent the electrostatic potential mapped on the Hirshfeld surface (different orientations). The 2D fingerprint plots (a–e), di and de represent the closest internal distance from a given point on the Hirshfeld surface and closest external contact, respectively.

dark golden-orange, orange, orange-red, deep-red crystal and solid forms of *trans*-$[Ru^{II}Cl_2(py)_4]$ and therefore, may appropriately be referred here to draw certain parallels and comparisons.

There were a few studies where *trans*-$[Ru^{II}Cl_2(py)_4]$ was reported to have formed from the residual filtrate or as a side-product of the main reaction. Robertson and coworkers,[39] reported an orange solid of *trans*-$[RuCl_2(C_5H_5N)_4]$ on concentration of a residual filtrate from the reaction of $[Ru_2(C_6H_6)_2Cl_3]PF_6$ with excess pyridine in ethanol. Also, they obtained the complex as a co-product on the prolonged reaction of $Cs[Ru(C_6H_6)Cl_3]$ in neat pyridine. Likewise, Ruiz-Ramirez *et al.*[40] obtained orange-red crystalline form as a primary product and also reported the formation of the complex as a side product.

In this study, the complex **C2** was obtained with a yield of 22% from the filtrate. Robertson *et al.*[39] reported a yield of 24% for their orange solid that was also obtained from filtrate, as stated earlier. Isolated as the primary product from a reaction, complex *trans*-$[RuCl_2(C_5H_5N)_4]$ was obtained as red blocks of crystals with 80% yield by Trivedi *et al.*,[25] Bu *et al.*[24] obtained it as yellow precipitate with a yield of 70.83% (0.34 g) while Wong *et al.*[22] obtained blocks of orange-red crystals with a substantially low yield of 42% and Elsegood *et al.*[23] did not report the yield of their red-block crystals.

Crystals of **C2** are quite hard, non-hygroscopic, stable in air for a very long time as was also reported by Trivedi *et al.*[25] It does not decompose or melt even at 300°C that indicates its strength of bonds. However, Robertson *et al.*[39] reported decomposition points of 255°C for their orange solid while Ruiz-Ramirez *et al.*[40] reported 270°C (D.P) for their orange-red crystalline complex. (see Table S10, Supplementary Information).

C2 is soluble in $CHCl_3$, CH_2Cl_2, DMSO, DMF and insoluble in petroleum ether similar to that reported by Trivedi *et al.*[25] Also, **C2** was found to be insoluble in water, organic solvents such as methanol, ethanol, hexane, etc. The molar conductance value of the complex suggests its non-conducting nature in dichloromethane as was also reported by Robertson *et al.*[39] for their orange solid.

The IR spectrum of complex **C2** shows an intense signal centered at 1623 cm^{-1} that is assigned to $\upsilon_{C=N}$ stretching frequency.[14] A low-intensity band observed at 557 cm^{-1} was assigned to υ_{Ru-N} (see Figure S7, Supplementary Information). These assignments were primarily made by correlation with the published work

of Malecki *et al.* on ruthenium(II) complexes, $[RuCl_2(C_6H_7N)_4]$.[14] Other prominent IR spectral peaks are given under analytical studies (section 2.4) of this paper. A comparison with the earlier reported peaks of the IR spectrum by Bu *et al.*[24] and Trivedi *et al.*[25] did not reveal any identical matching signals except the one at 2924 cm^{-1} (in Trivedi *et al.* paper) that is assigned to δ_{ring}. However, the signals presented here are seemingly close to those reported by Trivedi *et al.*[25] particularly, the signals in the regions, 1445, 800 and 759 cm^{-1} that are assigned to υ_{CH} and δring,[41] respectively. The strong broad band observed in the region 3690–3630 cm^{-1} centered at 3436 cm^{-1} indicates the presence of water molecules that may be due to the moisture absorbed by the hygroscopic KBr during pellet preparation.

The electronic absorption spectral profile of this brown colored complex **C2** shows absorptions at ~454–464 nm (100)(sh), 397 nm (400) and 275 nm (970) between 250–600 nm range using $CHCl_3$ solvent at a concentration of 1 mM. Here, the absorption at ~550–572 nm (ε = 6 $M^{-1}cm^{-1}$) is vaguely visible. However, at a higher concentration (~2.8 mM), the weak band at ~550–572 nm with ε = 60 $M^{-1}cm^{-1}$ was observable (see Figure S6, a&b, Supplementary Information). Thus, one can expect a more detectable absorption near ~550–572 nm in **C2** at higher concentrations and hence is concentration-dependent. The strong and sharp absorption in the UV-visible range of light at a wavelength (λ_{max}) of 275 nm is attributed to combined contributions from intraligand $\pi\rightarrow\pi^*$ and $n\rightarrow\pi^*$ transitions due to bonding and non-bonding electrons present in chlorine and pyridine ligands.[14] The other remaining bands fall in the visible range of light having a strong absorption centered at λ_{max} of 397 nm and a broad shoulder clearly visible at ~450–470 nm that are attributed to MLCT due to $d\rightarrow\pi_{py}^*$ excitation. These electronic spectral bands obtained for complex **C2** are similar to those observed in other octahedral ruthenium(II) complexes.[42] The broad and weak intensity band in the range 550–575 nm is assigned to d–d transition.[14,43,44]

Trivedi and coworkers[25] had reported two bands, one at a wavelength of 248 nm and other at 450 nm with ϵ_{max} of 23,535 and 53,761 $dm^3mol^{-1}cm^{-1}$, respectively for their red colored *trans*-$[Ru^{II}Cl_2(py)_4]$. They attributed the first band at 248 nm to intraligand π–π^* transition, while the second lower energy band centered at 450 nm was attributed to MLCT transition (see Table S10, Supplementary Information). On comparison with the absorption spectrum of complex **C2**, the band at 397 nm, was found to be blue-shifted by 53 nm while the peak at 275 nm was red-shifted by 27 nm having comparatively lower extinction coefficient values than the corresponding absorption peaks reported by Trivedi *et al.*[25] A summary of comparative studies, showing the UV-visible spectral bands reported for *trans*-$[Ru^{II}Cl_2(py)_4]$ in a few different studies are presented in Table S10 of Supplementary Information.

Signals in the ^{1}H NMR spectrum of this complex are assigned and presented under the analytical studies, section 2.4 of this paper and in Figure S8 of Supplementary Information. Trivedi *et al.*[25] had reported the signals at δ, 7.59 (m, 8H, J = 7.5 Hz), 7.40 (m, 4H, J = 6.0 Hz) and 7.38 (m, 8H, J = 6.9 Hz) ppm for their complex. On comparison with the ^{1}H NMR spectral signals of complex **C2**, small differences in positions and multiplicity of signals were found.

In the[13]C NMR spectrum, two signals were observed in the region between δ, 123–133.85 ppm that are assigned to the aromatic carbons on pyridine moiety. A signal at δ, 157.52 ppm is assigned to –C=N group.[45] The extra peaks in NMR spectra appear to be related to trace quantities of applied solvents. ^{13}C NMR spectral data for *trans*-$[RuCl_2(py)_4]$ was not available from literature to draw any comparisons. The signals in ^{13}C NMR spectrum of this complex are assigned and presented under the analytical studies, section 2.4 of this paper and in Figure S9 of Supplementary information.

The spectroscopic data of IR and ^{1}H NMR (Coe 2004)[15] and UV-visible (Coe *et al.*)[13] for dark-golden orange complex needs to be mentioned. The crystallinity and crystal data for their complexes were not reported in these papers. B J Coe and coworkers (1995)[13] reported four electronic spectral bands at 206 nm (ε = 29,000 $M^{-1}cm^{-1}$), 250 nm (ε = 15,700 $M^{-1}cm^{-1}$), 398 nm (ε = 25,100 $M^{-1}cm^{-1}$) and 450 (sh) nm (ε = 7,800 $M^{-1}cm^{-1}$) in the electronic spectrum of their dark golden-orange colored complex that was recorded in acetonitrile. The first and second band were assigned π–π^* transition while the third band and fourth, a shoulder were assigned to $d\pi$–π^* transitions. The dark golden-orange color of the complex was attributed to MLCT band at 398 nm with a low energy shoulder at 450 nm (see Table S10, Supplementary Information).

In another paper, B J Coe (2004)[15] reported the IR spectral data of their complex at ν_{max} of 1478, 1445, 759 and 690 cm^{-1} that matched with those of complex **C2**. The author also reported an absorption spectral band at 398 nm with ϵ_{max} of 24,000 $M^{-1}cm^{-1}$ recorded in CH_2Cl_2. However, another comparatively weaker band near ~240 nm (approx.) and a weak broad shoulder was seemingly observable near ~460 nm

(approx.) in the figure presented in the paper. The chemical shifts in the ^{1}H NMR spectral data of complex **C2** exhibited close similarity to those reported by the author with signals at δ, 8.63 (d, 8H, J = 5.1 Hz), 7.65 (t, 4H, J = 7.6 Hz) and 7.13 (t, 8H, 7.0 Hz) ppm in CD_2Cl_2.[13]

3.4 *Interpretation*

A summary of different reaction conditions for the preparation of *trans*-[$Ru^{II}Cl_2(py)_4$] is presented in Table S10 of Supporting Information. In prior reports, the block-shaped, yellow-brown,[17] yellow,[18] orange, red, or orange-red forms of *trans*-[$Ru^{II}Cl_2(py)_4$] were formed by different methods. Hence, it arises from these observations of various preparative methods and experimental conditions using different solvents like pyridine, methanol, ethanol, toluene, CH_2C1_2/CH_3CN, etc., for synthesis and crystallization process that the methanol, which was used as a solvent in the present study, may not have played a significant role in the physical alteration of **C2**.

The key point to note here is that the crystal-color morphology of the present form of *trans*-[$Ru^{II}Cl_2$(-py)$_4$] is distinct from the previously reported crystal forms and from the above-stated rationale to comprehend the process, it appears highly feasible that crystallization might have occurred in presence of bulky dihydrazone molecule in the filtrate medium that played a significant role. Correspondingly, the needle morphology of **C2** is attributed predominantly to the presence of the bulky molecule of bis(2-hydroxy-1-naphthaldehyde)adipoyldihydrazone in the medium that might have changed the course of crystallization of the complex and caused the difference in crystal habit. So analogous to an additive in a reaction mixture, it probably interfered with the crystal growth process and as a result, in this case, it has led to different growth rates of the individual faces on exposed crystal surfaces eventually lengthening the overall crystal shape resembling long and not so slender needles.

The distinct brown color in **C2** may be attributed to the combined contributions of the prominent absorptions, one at 397 nm and another in the range, ∼450–470 nm (sh) that are attributed to a charge transfer between the ligand donors and Ru(II) acceptor unit along with the other weak band between 550–575 nm that is assigned to the d–d transition band.

The intermolecular interactions in **C2** when compared with the block-shaped, red and orange-red crystal forms, have revealed the existence of different symmetry of intermolecular C—H···Cl interactions in crystal packing structure for **C2** as is mentioned under crystal description (Section 3.1) of this paper. The molecular interactions form a vast network between the packed molecules of the unit systems that result in packing interactions which stabilizes the crystal structure. The intermolecular interactions can influence crystal packing and relatably affect the structural units and consequently impact the electronic transitions.[46–50] In the absorption spectrum of this complex, the lower energy band at 397 nm was blue-shifted by 53 nm while the absorption peak at 275 nm was red-shifted by 27 nm with a comparatively lower extinction coefficient values with respect to the corresponding absorption peaks reported by Trivedi *et al.*[25] (using same solvent, $CHCl_3$). The appearance of a new weak broad band between 550–575 nm, probably is a consequence of the nature of packing interactions in **C2** that is subtly different from the past reports. Correspondingly, this indicates the influence of packing interactions on the physical and chemical properties[51,52] of the crystal revealing the resulting physicochemical change due to polymorphism.

It is the intermolecular and intramolecular interactions in the lattice that are ultimately manifested in physicochemical properties. Thus, taking into account that the geometries, bond lengths, bond angles and torsional angles of **C2** are subtly different from the previously reported crystal forms, it appears that the intra-molecular and inter-molecular interactions that govern the packing in solids play a significant role in influencing the changes. Considering, the existence of a different symmetry of intermolecular C—H···Cl interaction in **C2** that resulted in different crystal packing, we may unambiguously relate this with the distinguishable differences in its physical properties such as color, size, shape, etc. Hence, this leads to suggest that the difference in crystal packing has affected the change observed in the absorption spectra of this complex.

Further, the possibility of solvent affecting the distortion or destroying the crystal packing or the solvent effect on absorption spectra cannot be ignored or nullified in the solution phase absorption spectra. However, it may preferably remain underestimated here as the comparisons with the same solution-phase ($CHCl_3$) absorption spectra of the past report (Trivedi *et al.*[25]) draw an empirical correlation between the change in absorption spectra with their essential difference in packing arrangements. Several studies and literature have reported the impact of crystal packing on the absorption spectra in solution-phase of different polymorphs.[53,54]

These observations thus point towards how the bulky dihydrazone molecule present in the medium functioning as an additive (impurity) had affected the crystallization process, thereby modifying the molecular environment and resulting in different morphology, structural characteristics and properties of the crystal **C2**.

3.5 *Antibacterial activity and toxicity studies*

Ruthenium-based complexes are known to show biological activity having anticancer, antibacterial and antiviral properties.[55] As antibacterials, some polypyridyl ruthenium(II) complexes exhibited MICs as low as 2 μg mL^{-1} against Gram-positive strains; they, however, showed inactivity towards Gram-negative bacteria.[56]

On considering the bioavailability in contrast to minimum bactericidal concentration values for many ruthenium complexes, the uptake was found to be considerably less in Gram-negative bacteria compared to Gram-positive species.[56] Gorle *et al*. reported uniform to or greater level of cellular uptake of tri-nuclear and tetra-nuclear ruthenium(II) complexes in Gram-negative bacteria compared to Gram-positive bacteria. However, Gram-negative species showed lower activity which was inferred to as due to their inherent resistance to these complexes, especially *Pseudomonas aeruginosa*.[57,58] Similar results were obtained by Matshwele *et al.* for their mononuclear compounds of ruthenium and polypyridyl ligands that showed better antibacterial efficacy for Gram-positive *S. aureus* and MRSA bacteria compared to the Gram-negative *K. pneumoniae* bacteria.[55] The general trend of ruthenium(II) complexes to show potent activity for Gram-positive bacteria compared to Gram-negative bacteria was interpreted as due to the less restrictive membrane in Gram-positive bacteria.[55]

In consonant with the aforementioned studies, the complex **C2** has shown no antibacterial activities towards Gram-negative bacteria *E. coli* and *K. pneumoniae*, but was more effective on the Gram-positive, methicillin-resistant *S. aureus.* The zone of inhibition of 8.3 ± 0.17 mm at 60 μg indicates modest antibacterial activity of the complex against *S. aureus*. The antibiotic resistance profile of the clinical isolates are presented in Table 3, Figure 4 and Figure S3 of Supplementary Information. To the best of our knowledge, so far, there has been no literature report pertaining to the biological activity of *trans*-$[Ru(py)_4(Cl)_2]$.

The mechanism of inhibition in bacterial growth showed by the complex and its probable cytotoxicity analysis *in vitro* is yet to be studied. However, preliminary investigations in rats *in vivo* showed that the complex does not produce any known toxic effect within the given test period and drug dose (see S4 and S5, Supplementary Information).

3.6 *Docking studies*

The ruthenium complexes show a potent binding ability to nucleic acid and protein.[56] As antimicrobials, many findings on polypyridyl octahedral ruthenium(II) complexes suggest DNA binding in these complexes.[58] These ruthenium complexes have been widely studied, mainly focussing on their anticancer activities. To date, the two ruthenium complexes, KP1019 and KP1339 that were proved to display promising anticancer activities have entered clinical trials.[59–61] Based on such reports, the molecular docking for complex **C2** was computed and performed to find the putative binding geometry with target protein to access the antibacterial activities. The molecular docking of complex **C2** with ATP*Sa* was performed. **C2** hydrogen bonds with Glu58 of the ATP*Sa* (Figure 5) and the gold score for this docking was found to be 37.10 and the distance between the Glu58 and ATP*Sa* was 3.226 Å.

4. Conclusions

Tetragonal *trans*-dichlorotetrakis(pyridine-*N*)ruthenium(II) formed by slow evaporation of filtrate from a reaction mixture, exhibited brown color and needle (acicular) morphology different from previously reported orange-red and red crystals with block morphology. This apparent increase in dimension of up to 12 mm × 1.2 mm for **C2** is probably due to different rates of self-assembling on individual crystal faces during crystal growth that may have been affected by the significant influence of comparatively large dihydrazone molecule present in the medium which may have modified the interaction process of solvent–solute and the crystal surface.

The crystallographic and spectroscopic data of this complex were examined, analyzed and compared with past reported structures. It was found that although its molecular structure is in good agreement with the ones reported earlier, it is not entirely similar, having subtle differences in cell parameters and spectral features. It was also found to have a subtle difference in symmetry of C—H···Cl intermolecular interaction in the crystal packing from previously discussed structures. The

Table 3. Zone of inhibition (in mm) of complex **C2** against the clinical bacterial isolates.

Clinical isolate	Antibiotics resistant to	Average zone of inhibition (mm)*
Gram-negative isolates		
Escherichia coli		ND
	Ampicillin, cefepime, cefoperazone, cefepime, ertapenem, meropenem, kanamycin, nalidixic acid, aztreonam, ceftazidime, cefotaxime	
Klebsiella pneumoniae		ND
	Ampicillin, cefepime, cefoperazone, cefixime, imipenem, ertapenem, meropenem, kanamycin, cefoxitin, nalidixic acid, aztreonam, ceftazidime, cefotaxime	
Gram-positive isolate		
Staphylococcus aureus		8.3 ± 0.17
	Oxacillin, methicillin, cefepime, cefotaxime, ceftaxidime, cefoperazone,cefotoxime, cefdiner	

*Inclusive of well diameter (6 mm); ND, not detected.

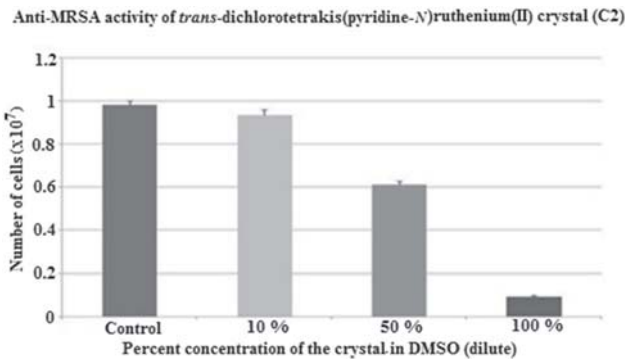

Figure 4. Inhibition of methicillin-resistant *S. aureus* tested by microdilution broth test; with reference to the control, **C2** inhibits growth at different concentrations. (key: control comprise 5% DMSO, 100% is 1000 μg/mL, 50% is 500 μg/mL and 10% is 100 μg/mL).

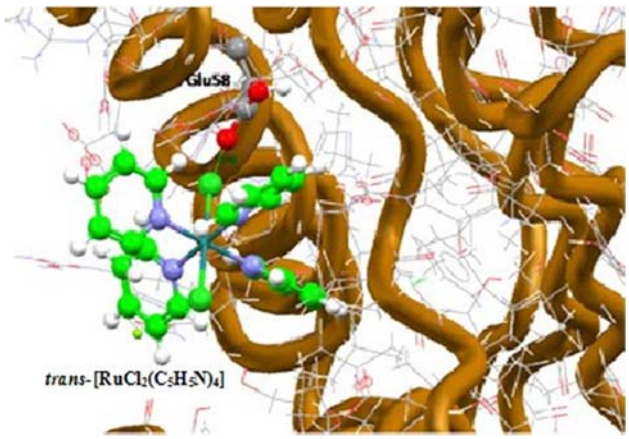

Figure 5. The title molecule (*trans*-$[RuCl_2(C_5H_5N)_4]$: Ball and stick model) is hydrogen-bonded (green dots) with the Glu58 residue (ball and stick model) of ATP*Sa* (tube representation).

crystal and molecular structure of the complex are stabilized by weak intercontacts having contributions majorly from H···H towards Hirshfeld surfaces.

The packing interactions can significantly affect the physical, mechanical, chemical, optical, or electrical properties of a crystal. Hence, it follows that the reorganization of molecular interactions with subtly different packing interactions probably has, in this case, caused the morphological change and has also induced the color difference.

In summary, this study reports the change in shape, size and color morphology of *trans*-$[RuCl_2(py)_4]$. Through the analysis of different investigations, we have studied a few different properties of **C2** that visibly has different physical attributions from the previously reported crystal forms. Here, we have attempted to understand the role of an additive or impurity in affecting the crystal habit. Apparently, it is noticeable that the elongated size of crystal **C2** is influenced by the probable presence of another large-sized dihydrazone molecule in the filtrate medium that appears to have performed like an impurity/additive. Furthermore, these long crystals also have subtly different crystal packing interactions from all the previous structurally similar crystal forms that have affected the structural units of the system resulting in the difference of color.

Further, the biological aspects revealed non-toxicity and antimicrobial activity against pathogen *S. aureus*. This antibacterial potential has been screened through molecular docking studies that have revealed that **C2** hydrogen bonds with Glu58 of the ATP*Sa* and the gold score for this docking is found to be 37.10.

Supplementary Information (SI)

Following additional informations for the complex **C2** are available in Supplementary Information, (S1) CCDC No. 997152 in Crystallographic data centre (e-mail: deposit@ccdc.ac.uk or http://www.ccdc.cam.ac.uk), (S2) Table S2(a), Selected geometric parameters (Å, °); Table S2(b), Selected Bond Angles (°); Table S2(c), Selected Torsional Angles (°); Table S2(d), Comparison of selected geometric parameters (Å, °) and crystal data collection temperature for crystal forms in the cited past reports, (S3) Antibacterial activity study; Figure S3 for Inhibition zone show antibacterial activity against *S. aureus* of complex, (S4) Toxicity analysis of complex, (S5) Table S5, *In vivo* toxicity studies, (S6) Figures S6 (a and b) for UV-visible spectra of complex, (S7) Figure S7 for IR spectrum of complex, (S8) Figure S8 for ^{1}H NMR spectrum of complex, (S9) Figure S9 for ^{13}C NMR spectrum of complex, (S10) Table S10 for Summary of reaction for preparation of *trans*-[$RuCl_2(py)_4$] by different methods (using different reagents and solvents), its color and UV-Visible absorption bands, (S11) CIF data (S12), checkCIF file.

Acknowledgments

We are highly indebted to Prof. A T Khan, the Vice-Chancellor of Aliah University, Kolkata and Prof. R A Lal, Department of Chemistry, North-Eastern Hill University, Shillong for their helpful discussions. Thanks are also due to the Head Incharge and Mr. Chandan Buragohain of CIF, IIT-Guwahati, Guwahati for recording NMR spectra. We are thankful to Dr. Pranjal Saikia, Dr. Samiul Haque and Nabajyoti Dhing from Department of Applied Sciences, Gauhati University, Guwahati for their help recording electronic and IR spectra. We thank the Head, USIC, Gauhati University, Guwahati for recording the crystallographic data. M K S thanks IOE and DST PURSE, University of Mysore, Mysuru. P. S. and P. M. are thankful to MHRD, Govt. of India assisted by the World Bank for TEQIP-III project grants.

References

1. Dandekar P, Kuvadia Z B and Doherty M F 2013 Engineering crystal morphology *Annu. Rev. Mater. Res.* **43** 359
2. Sudha C and Srinivasan K 2014 Understanding the effect of solvent polarity on the habit modification of monoclinic paracetamol in terms of molecular recognition at the solvent crystal/interface *Cryst. Res. Technol.* **49** 865
3. Smith P E 2010 The effect of urea on the morphology of NaCl crystals: A combined theoretical and simulation study *Fluid Phase Equilib*. **290** 36
4. Keraliya R A, Soni T G, Thakkar V T and Gandhi T R 2010 Effect of solvent on crystal habit and dissolution behavior of tolbutamide by initial solvent screening *Dissolution Technologies* **17** 16
5. Braga D, Grepioni F, Maini L and Polito M 2009 Crystal polymorphism and multiple crystal forms *Struct. Bond.* **132** 25
6. Chen J, Lin L, Song Y and Shao L 2009 Influence of KOH on the hydrothermal modification of $Mg(OH)_2$ crystals *J. Crystal Growth* **311** 2405
7. Wang D X, Chen S S, Li Y Y, Yang J Y, Wei T Y and Jin S H 2014 An Investigation into the effects of additives on crystal characteristics and impact sensitivity of RDX *J. Energ. Mater.* **32** 184
8. Weissbuch I, Addadi L, Lahav M, and Leiserowitz L 1991 Molecular recognition at crystal interfaces *Science* **253** 637
9. Hendriksen B A, Grant D J W, Meenan P and Green D A 1998 Crystallisation of paracetamol (acetaminophen) in the presence of structurally related substances *J. Cryst. Growth* **183** 629
10. Tedesco E, Giron D and Pfeffer S 2002 Crystal structure elucidation and morphology study of pharmaceuticals in development *Cryst. Eng. Comm.* **4** 393
11. Evans I P, Spencer A and Wilkinson G 1973 Dichlorotetrakis(dimethyl sulphoxide)ruthenium(II) and its use as a source material for some new ruthenium(II) complexes *J. Chem. Soc.*, *Dalton. Trans.* **2** 204
12. Wu X L, Ye R F, Jia A Q, Chen Q and Zhang Q F 2013 *trans*-Dibromidotetrakis (pyridine-κN) ruthenium(II) *Acta Cryst*. **E69** m105
13. Coe B J, Meyer T J and White P S 1995 Synthetic and structural studies on *trans*-Tetrapyridine Complexes of Ruthenium(II) *Inorg. Chem.* **34** 593
14. Małecki J G, Jaworska M, Kruszynski R and Gilbortnowska R 2005 Synthesis and characterization of [$RuCl_2$(picoline)$_4$] complexes: Crystal structure of [$RuCl_2$(ß-pic)$_4$] *Polyhedron* **24** 445
15. Coe B J 2004 Syntheses and characterization of ruthenium(II) tetrakis(pyridine) complexes, An advanced coordination chemistry experiment or mini-project *J. Chem. Edu.* **8** 5
16. Gilbert J D, Rose D and Wilkinson G 1970 Preparative use of blue solutions of Ruthenium(II): Ruthenium-(II) and -(III) complexes with amines, nitriles, phosphines, *etc. J. Chem. Soc. A* 2765
17. Bottomley F and Mukaida M 1982 Electrophilic behaviour of nitrosyls: preparation and reactions of Six-co-ordinate Ruthenium Tetra(pyridine) Nitrosyl Complexes *J. Chem. Soc. Dalton Trans.* 1933
18. Nagao H, Nishimura H, Kitanaka Y, Howell F S, Mukaida, M and Kakihana H 1990 Selective formation of Ruthenium(IV) complexes with a monooxygen ligand: *trans*-$[RuX(O)(py)_4]^+$ (X = Cl, ONO) *Inorg. Chem*. **29** 1693
19. Basumatary D, Lal R A and Kumar A 2015 Synthesis and characterization of low- and high-spin manganese(II) complexes of polyfunctional adipoyldihydrazone: Effect of coordination of N-donor ligands on stereo-redox chemistry *J. Mol. Struct.* **1092** 122
20. Lal R A, Basumatary D, Chanu O B, Lemtur A, Asthana M., Kumar A and De A K 2011 Synthesis, characterization, reactivity and electrochemical studies of

manganese(IV) complexes of bis(2-hydroxy-1-naphthaldehyde)adipoyldihydrazone *J. Coord. Chem*. **64** 300
21. Basumatary Debajani 2008 *Synthesis and Structure of Manganese and Ruthenium complexes derived from some Adipoyl Dihydrazones* (North-Eastern Hill University, Shillong, India) 105
22. Wong W T and Lau T C 1994 *trans*-Dichlorotetrapyridineruthenium(II) *Acta Cryst.* **C50** 1406
23. Elsegood M R J and Tocher D A 1995 *trans*-Dichlorotetrakis(pyridine-*N*)ruthenium(II) *Acta Cryst.* **C51** 40
24. Bu Z, Wang Z, Yang L and Cao S 2010 Synthesis of propylene carbonate from carbon dioxide using *trans*-dichlorotetrapyridineruthenium(II) as catalyst *Appl. Organomet. Chem.* **24** 813
25. Trivedi M, Sharma Y K, Nagarajan R and Rath N P 2010 Synthetic, spectral and structural study of mono bis(pyridine)dichlorobis(dimethyl sulfoxide-S) ruthenium(II) complex, $[RuCl_2(py)_2(dmso\text{-}S)_2]$ and its reactivity with nitrogen donor bases in polar and non-polar solvent *J. Mol. Struct.* **975** 335
26. Lam P L, Lu G L, Hon K M, Lee K W, Ho C L, Wang X, Tang J C O, Lam K H, Wong R S M, Kok S H L, Bian Z X, Li H, Lee K K H, Gambari R, Chui C H and Wong W Y 2014 Development of ruthenium(II) complexes as topical antibiotics against methicillin resistant *Staphylococcus aureus Dalton Trans.* **43** 3949
27. Caruso F, Monti E, Matthews J, Rossi M, Gariboldi M B, Pettinari C, Pettinari R and Marchetti F 2014 Synthesis, characterization, and antitumor activity of water-soluble (arene)ruthenium(II) derivatives of 1,3-dimethyl-4-acylpyrazolon-5-ato ligands. First example of Ru(arene)(ligand) antitumor species involving simultaneous Ru−N7(guanine) bonding and ligand intercalation to DNA *Inorg. Chem*. **53** 3668
28. Fernandez L and Hancock R E W 2012 Adaptive and mutational resistance: Role of porins and efflux pumps in drug resistance *Clin. Microbiol. Rev.* **25** 661
29. Siemens 1994 *XSCANS User's Manual and XEMP* Siemens Analytical X-ray Instruments Inc., Madison, Wisconsin, USA; Farrugia L J 1998 *ORTEP-32 for Windows*, University of Glasgow, Scotland
30. Sheldrick G M 1997 *SHELXS97, SHELXL97 and CIFTAB*, University of Gottingen, Germany
31. Macrae C F, Bruno I J, Chisholm J A, Edgington P R, McCabe P, Pidcock E, Rodriguez-Monge L, Taylor R., Streek J van de and Wood P A 2008 Mercury CSD 2.0 – new features for the visualization and investigation of crystal structures *J. Appl. Crystallogr*. **41** 466
32. Wolff S K, Grimwood D J, McKinnon J J, Jayatilaka D and Spackman M A 2007 *Crystal Explorer 3.0*. University of Western Australia, Perth
33. Spackman M A and McKinnon J J 2002 Fingerprinting intermolecular interactions in molecular crystal *Cryst. Eng. Comm.* **4** 378
34. Kumar S M, Manjunath B C, Lingaraju G S, Abdoh M M M, Sadashiva M P and Lokanath N K 2013 A Hirshfeld surface analysis and crystal structure of 2'-[1-(2-fluoro-phenyl)-1H-tetrazol-5-Yl]-4-methoxy-biphenyl-2-carbaldehyde *Cryst. Struct. Theory Appl.* **2** 124
35. Spackman M A, McKinnon J J and Jayatilaka D 2008 Electrostatic potentials mapped on Hirshfeld surfaces provide direct insight into intermolecular interactions in crystals *Cryst. Eng. Comm.* **10** 377
36. Reller L B, Weinstein M, Jorgensen J H and Ferraro M J 2009 Antimicrobial susceptibility testing: a review of general principles and contemporary practices *Clin. Infec. Dis*. **49** 1749
37. Sadowski J, Gasteiger J and Klebe G 1994 Comparison of automatic three-dimensional model builders using 639 X-ray structures *J. Chem. Inf. Comput. Sci*. **34** 1000
38. Cole J C, Nissink J W M and Taylor R 2005 Protein-ligand docking and virtual screening with GOLD. In *Virtual Screening in Drug Discovery* Shoichet B, and Alvarez J (Eds.) (Boca Raton, F L: Taylor & Francis Group) 379
39. Robertson D R, Stephenson T A and Arthur T 1978 Cationic, Neutral and Anionic Complexes of Ruthenium(II) containing η^6-Arene Ligands *J. Organomet. Chem.***162** 121
40. Ruiz-Ramirez L, Stephenson T A and Switkes E S 1973 New Ruthenium(III) and Ruthenium(II) Complexes containing Triphenylarsine and -phosphine and Other Ligands *J. Chem. Soc. Dalton Trans.* 1770
41. Nakamoto K 1986 In *Infrared and Raman spectra of inorganic and coordination compounds* (New York: John Wiley and Sons) 978
42. Il'in M A, Emel'yanov V A and Baidina I A 2008 Structure and synthesis of nitrosoruthenium *trans*-diammines $[Ru(NO)(NH_3)_2Cl_3]$ and $[Ru(NO)(NH_3)_2(H_2O)Cl_2]Cl{\cdot}H_2O$ *J. Struct. Chem*. **49** 1090
43. Gowri S, Muthukumar M, Krishnaraj S, Viswanathamurthi P, Prabhakaran R and Natarajan K 2010 Ruthenium(II) unsymmetrical N_2O_2 tetradentate Schiff-base complexes: synthesis, characterization and catalytic studies *J. Coord. Chem.* **63** 524
44. Makhinya A N, Il'in M A, Baidina I A, Plyusnin P E, Alferova N I and Pishchur D P 2014 Structure, synthesis, and thermal properties of *trans*-$[Ru(NO)(NH_3)_4(SO_4)]NO_3{\cdot}H_2O$ *J. Struct. Chem.* **55** 311
45. Sathiyaraj S, Ayyannan G and Jayabalakrishnan C 2014 Synthesis, spectral, DNA binding and cleavage properties of ruthenium(II) Schiff base complexes containing $PPh_3/AsPh_3$ as co-ligands *J. Serb. Chem. Soc.* **79** 151
46. Chen P Y, Zhang L, Zhu S G and Cheng G B 2017 Role of intermolecular interaction in crystal packing: A competition between halogen bond and electrostatic interaction *J. Mol. Struct.* **1131** 250
47. Taylor R 2014 Which intermolecular interactions have a significant influence on crystal packing? *CrystEngComm.* **16** 6852
48. Fu F, Liao K, Ma J, Cheng Z, Zheng D, Gao L, Liu C, Li S and Li W 2019 How intermolecular interactions influence electronic absorption spectra: insights from the molecular packing of uracil in condensed phases *Phys. Chem. Chem. Phys.* **21** 4072
49. He X, Benniston A C, Saarenpaa H, Lemmetyinen H, Tkachenko N V and Baisch U 2015 Polymorph crystal packing effects on charge transfer emission in the solid state *Chem. Sci.* **6** 3525
50. Kasuga N C, Saito Y, Sato H and Yamaguchi K 2015 Packing polymorphism in the crystal structure of 4,5-dimethoxy-2-nitrobenzyl acetate *Acta Cryst. E* **71** 483

51. Pratik S M, Nijamudheen A, Bhattacharya S and Datta A 2014 Color polymorphism: Understanding the diverse solid-state packing and color in dimethyl-3,6-dichloro-2, 5-dihydroxyterephthalate *Chem. Eur. J*. **20** 3218
52. Yang J, Zhen X, Wang B, Gao X, Ren Z, Wang J, Xie Y, Li J, Peng Q, Pu K and Li Z 2018 The influence of the molecular packing on the room temperature phosphorescence of purely organic luminogens *Nat. Comm.* **9** 1
53. Cárdenas J C, Aguirre-Díaz L M, Galindo J F, Alí-Torres J, Ochoa-Puentes C, Echeverri M, Gómez-Lor B, Monge M Á, Gutiérrez-Puebla E and Sierra C A 2019 Nature of color diversity in phenylenevinylene-based polymorphs *Cryst. Growth Des.* **19** 3913
54. Zhu Q, Zhang Y, Nie H, Zhao Z, Liu S, Wong K S and Tang B Z 2015 Insight into the strong aggregation-induced emission of low-conjugated racemic C6-unsubstituted tetrahydropyrimidines through crystal-structure–property relationship of polymorphs *Chem. Sci.* **6** 4690
55. Matshwele J T P, Nareetsile F, Mapolelo D, Matshameko P, Leteane M, Nkwe D O and Odisitse S 2020 Synthesis of Mixed Ligand Ruthenium(II/III) complexes and their antibacterial evaluation on drug-resistant bacterial organisms *J. Chem*. **2020** 1
56. Li F, Collins J G and Keene F R 2015 Ruthenium complexes as antimicrobial agents *Chem. Soc. Rev*. **44** 2529
57. Gorle A K, Feterl M, Warner J M, Wallace L, Keene F R and Collins J G 2014 Tri- and tetra-nuclear polypyridyl ruthenium(II) complexes as antimicrobial agents *Dalton Trans.* **43** 16713
58. Yang Y, Liao G and Fu C 2018 Recent Advances on Octahedral Polypyridyl Ruthenium(II) complexes as antimicrobial agents *Polymers (Basel)* **10** 650
59. Tang B, Shen F, Wan D, Guo B H, Wang Y J, Yi Q Y and Liu Y J 2017 DNA-binding, molecular docking studies and biological activity studies of ruthenium(II) polypyridyl complexes *RSC Adv.* **7** 34945
60. Bratsos I, Jedner S, Gianferrara T and Alessio E 2007 Ruthenium anticancer compounds: challenges and expectations *Chimia* **61** 692
61. Meng X, Leyva M L, Jenny M, Gross I, Benosman S, Fricker B, Harlepp S, Hebraud P, Boos A, Wlosik P, Bischoff P, Sirlin C, Pfeffer M, Loeffler J P and Gaiddon C 2009 A Ruthenium-containing organometallic compound reduces tumor growth through induction of the endoplasmic reticulum stress gene CHOP *Cancer Res.* **69** 5458